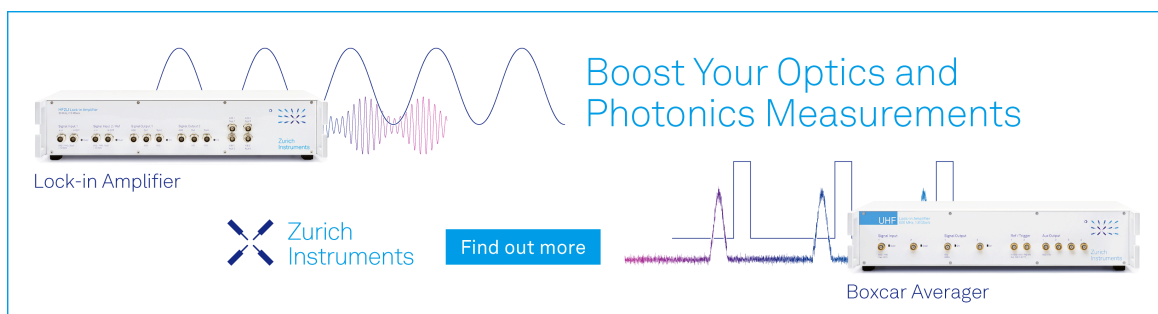# Virtual photon exchange vs electron transfer in interparticle Coulombic electron capture

Vincent Graves ⓘ ; Jan Šenk ⓘ ; Přemysl Kolorenč ⓘ ; Nicolas Sisourat ⓘ ; Jimena D. Gorfinkiel ✉ ⓘ

Check for updates

View Online   Export Citation

Virtual photon exchange vs electron transfer in interparticle Coulombic electron capture

Vincent Graves,[1,a] (iD) Jan Šenk,[2,3] (iD) Přemysl Kolorenč,[3] (iD) Nicolas Sisourat,[2] (iD) and Jimena D. Gorfinkiel[1,b] (iD)

AFFILIATIONS

[1] School of Physical Sciences, The Open University, Milton Keynes, United Kingdom
[2] Sorbonne Université, CNRS, Laboratoire de Chimie Physique-Matière et Rayonnement, F-75005 Paris, France
[3] Institute of Theoretical Physics, Faculty of Mathematics and Physics, Charles University, Prague, Czech Republic

[a] Electronic mail: vincent.graves@open.ac.uk
[b] Author to whom correspondence should be addressed: jimena.gorfinkiel@open.ac.uk

ABSTRACT

We have investigated Interparticle Coulombic Electron Capture (ICEC) using an *ab initio* approach for two systems, $H^+ + H_2O$ and $H + H_2O^+$. In this work, we have determined the contribution of virtual photon exchange and electron transfer to the total ICEC cross section as a function of the distance between the charged and neutral particles. Furthermore, we have shown that the relative orientation of the electron acceptor and neighbor systems affects the magnitude of the ICEC cross sections by at least two orders at relatively small distances. This geometry dependence, present even for distances as large as 10 a_0, is due to the electron transfer contribution. The relative magnitude of each contribution to ICEC seems to depend on the system studied. By replacing the projectile electron with a positron, we have confirmed that electron transfer also takes place in positron collisions and that the charge of the projectile has a noticeable effect on the process, particularly at low scattering energies.

I. INTRODUCTION

Interparticle Coulombic Electron Capture (ICEC) is an environment enabled process[1] that takes place when an electron is captured by an atom, a molecule, or a quantum dot; the excess energy is then released, leading to the ionization or excitation of a nearby particle. The process was first predicted and quantified using an analytical approach that provides reliable cross sections when the electron acceptor and neighbor systems are far apart.[2,3]

Electron capture plays an important role in a number of applied science areas, from plasma physics to biology. As with all processes initiated by a free electron, gas phase (and the theoretical equivalent, isolated target) studies significantly outweigh those where the target/acceptor is embedded in an environment. However, many of the applied areas of interest, in particular radiation interaction with biological matter,[4] involve condensed or loosely bound systems. The importance of ICEC in these areas is not yet understood, but since the process leads to both changes in the species present and, in the case of ionization, a change to the kinetic energy distribution of electrons, it has the potential to significantly affect, for example, energy deposition.

In addition to the transfer of a virtual photon, the same collision induced outcome is achieved if the transfer of an electron takes place. In the former, the acceptor captures the electron and emits the virtual photon, while in the latter, it is the environment that provides the electron and no capture of the projectile electron takes place. These mechanisms are labeled "direct" and "exchange," respectively, in the original ICEC publications.[2,3] The two mechanisms are shown schematically in Fig. 1. Cross sections calculated with our approach model both contributions, and we will refer to them, for simplicity, as **total** ICEC cross sections, even when one contribution dominates.

These two contributions have also been identified in Interatomic Coulombic Decay (ICD), another of a family of processes that involve the transfer of energy and/or charge between atoms/molecules through Coulombic interactions.[5] In ICD, as one
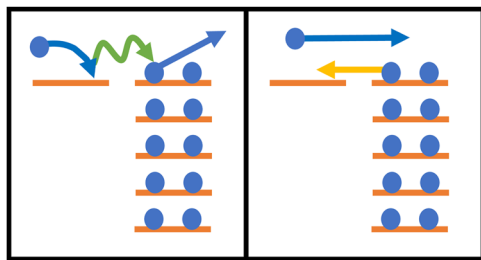
FIG. 1. Schematic depiction of the virtual photon exchange (left) and electron transfer (right) processes for H$^+$ + H$_2$O. The blue dots are electrons, and the arrows indicate an electron attached from, emitted into or moving in the continuum (blue), an electron moving between bound states (yellow), and a virtual photon (green). See the text for more details.

would expect, the charge exchange is predominant when the distance between the involved particles is shorter, whereas the virtual photon transfer dominates at longer distance.[6] The two contributions can be experimentally distinguished for certain systems in the case of ICD.[7–9]

In this work, we have performed *ab initio* ICEC cross section calculations to investigate the dependence of the two contributions on the distance between particles and their relative orientation. We have studied ICEC as a function of R, the distance between the acceptor and its neighbor for two processes:

- e$^-$ + H$^+$ + H$_2$O → H + H$_2$O$^+$ + e$^-$ ICEC-P
- e$^-$ + H + H$_2$O$^+$ → H$^+$ + H$_2$O + e$^-$ ICEC-W

with the initial cation and the neutral system in their respective electronic ground state. Calculations have been performed for two C$_{2v}$ geometries (shown in Fig. 2). The equilibrium geometry of the ground state of H$_2$O has been used in all calculations. In the rest of this article, we use the following notation: H$_2$O–H denotes the geometry with H$^{(+)}$ on the O side of water (left image in Fig. 2), and H–H$_2$O denotes the geometry with H$^{(+)}$ on the H$_2$ side of water (right image in Fig. 2).

We have used the R-matrix method for low-energy lepton scattering[10,11] as implemented in the UKRmol+ suite[12] to perform our calculations. The method has been applied before to the study of ICEC,[13–15] including the process labeled ICEC-P, for the H$_2$O–H geometry only. We have performed calculations both including and excluding exchange between the projectile and the target (see below) in order to differentiate the electron transfer and virtual
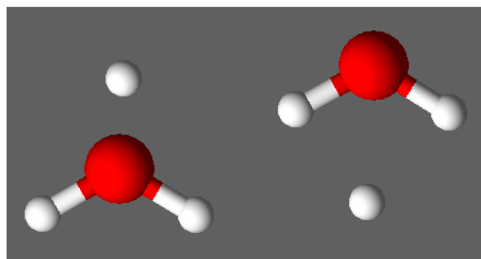

FIG. 2. Two geometries used in the calculations. Left: H$_2$O–H; right: H–H$_2$O.

photon exchange processes. We have also performed electron transfer calculations with a positron as the projectile: these calculations show that the charge of the projectile influences the electron transfer cross sections but has a smaller effect as the projectile energy increases.

A very recent review[1] summarizes the current understanding of ICEC; we note that at the moment, there is no experimental confirmation of the processes.

II. THE R-MATRIX METHOD

The R-matrix method is a well-established computational approach for the study of low energy electron–molecule/small cluster scattering. The method is usually applied, as it is here, within the fixed-nuclei approximation: the nuclei are assumed to be fixed in space while the electronic process takes place. Both elastic scattering and electronic excitation, as well as resonance formation, can be studied. In the case of ICEC, the final state of the system corresponds to electronic excitation channels. The UKRmol+ suite can also be used to study low energy positron scattering with molecules (see, for example, Refs. 16 and 17), where there is no exchange between the projectile and the target electrons.

The details of the method can be found elsewhere,[10,11] so we only briefly outline it below. The main idea of the approach is the division of space into two regions separated by a sphere defined by the R-matrix radius. In the inner region, exchange (if applicable) and correlation are crucial and the wavefunction for the system is expanded using a close-coupling approach,

$$\Psi_k^\Gamma(x_1,\ldots,x_{N+1}) = \mathscr{A} \sum_{i=1}^{n_b} \sum_{j=1}^{n_{c,i}} \Phi_i(x_1,\ldots,x_N)\gamma_{ij}(x_{N+1})a_{ijk}$$
$$+ \sum_{i=1}^{m} \chi_i^\Gamma(x_i,\ldots,x_{N+1})b_{ik}. \tag{1}$$

Here, x_i denotes the spin and space coordinates of the electron i and Γ denotes a specific irreducible representation. The functions $\Phi_i(x_1,\ldots,x_N)$ describe the target electronic states and γ_{ij} are continuum orbitals describing the projectile. The operator $\mathscr{A}$ ensures antisymmetrization of the wavefunctions when required; like Φ_i, the L^2 functions χ_i^Γ, which describe the short range correlation, are built as antisymmetrized products of bound molecular orbitals. The coefficients a_{ijk} and b_{ik} are determined through the diagonalization of the Hamiltonian matrix in the inner region.

In the outer region, the projectile is distinguishable from the target electrons and correlation is negligible. The wavefunction for the system has a simpler expression and can be obtained from solving a set of coupled differential equations. The $\Psi_k^\Gamma(x_1,\ldots,x_{N+1})$ and their eigenvalues are used to build an R-matrix at the boundary between the inner and outer regions. The R-matrix is then used as boundary conditions to solve the outer region problem using a propagation technique. The solutions are matched to known asymptotic expression from which scattering matrices can be obtained. From these, the integral cross sections are determined.

A. Computational details

Using previous target models[15] as a starting point, we improved the target wavefunctions $\Phi_i(x_1,\ldots,x_N)$ to ensure the correct order of the states at a large distance R. The best set of excitation thresholds

for the states of interest were obtained using the cc-pVDZ basis set, Hartree–Fock orbitals (calculated with MOLPRO[18]), and a complete active space model with an (8,9) active space. Therefore, in our calculations, the $1a_1$ orbital is frozen and $2a_1$, $1b_2$, $3a_1$, $1b_1$, $4a_1$, $5a_1$, $6a_1$, $2b_2$, $7a_1$ are active orbitals. Molecular orbitals $4a_1$ and $6a_1$ roughly correspond to the 1s and 2s orbitals on H/H$^+$.

The 20 states [$n_b = 20$ in Eq. (1)] included in the scattering calculation are listed in Table I. Comparison of the energies for R = 25 Å with the asymptotic ones shows that accurate excitation thresholds. For higher states, the thresholds are at least 2 eV too big. For this reason, we only present results up to 7 eV.

The R-matrix radius was set to 20 a_0. Only B-spline orbitals[12,25] were used to build the continuum orbitals γ_{ij}: 20 per l, with $l_{max} = 6$, of order 6. The highest partial wave included in the Legendre expansion of the integrals[12] was set to 85 for the one-electron and 30 for the two-electron ones.

Since rotation and vibrational motion are neglected in this study, ICEC is the only possible process, apart from elastic scattering, in the energy range of the calculations for ICEC-P. In the case of ICEC-W, the electronic excitation of H_2O^+ and dissociative recombination are also possible. The former is included in our calculations but the latter is not.

B. Separating the electron transfer contribution

In the UKRmol+ suite, it is possible to switch off the exchange between the projectile and the electrons of the target. This corresponds to removing the antisymmetrization operator from Eq. (1), and it is carried out in practice by setting the contributions to the inner region Hamiltonian matrix that arise from particle indistinguishability to zero. This has been implemented to study positron scattering. In addition, in order to run positron calculations, one needs to change the sign of the one-electron integrals, allow the positron to occupy orbitals already doubly occupied by target electrons, and ensure that the positron does not couple electronic states of different spins.[11,26]

We can use the switching off of exchange to get further insights into ICEC-P and ICEC-W. When exchange between projectile and target is switched off, the electron that comes in must be the electron that goes out (i.e., incoming and outgoing electrons are the same). This mean that, in fact, *there is no electron capture*: if the positive charge "moves" from the acceptor to the neighbor, this must be because an electron has been transferred from the neighbor to the acceptor. If we perform R-matrix calculations switching off exchange, then we are calculating, to a good approximation, an electron transfer cross section, $\sigma^{e\,transfer}$. This approach does not account for all contributions to the electron transfer process, however. For instance, exchange will play a role if the projectile is attached via the formation of a resonant state and is then ejected while an electron from the neighbor is transferred. Similarly, after an attachment, a different electron can be ejected from the water molecule in ICEC-W accompanied by an electron transfer; such a pathway is not included. However, the contribution of these mechanisms is likely to be very small and have a small effect on $\sigma^{e\,transfer}$, particularly in

TABLE I. Target state energies, in eV, relative to the lowest state for the R distance and geometry indicated. The asymptotic energies, determined from the published data,[19–24] are also tabulated.

| | Symmetry | State | R = 3 Å | | R = 8 Å | | R = 25 Å | | R = ∞ |
			H$_2$O–H	H–H$_2$O	H$_2$O–H	H–H$_2$O	H$_2$O–H	H–H$_2$O	
1	$^3B_1$	H(1s) H$_2$O$^+$($\tilde{X}\,^2B_1$)	0.0000	0.0000	0.0000	0.0000	0.0000	0.0000	0.0000
2	$^1B_1$	H(1s) H$_2$O$^+$($\tilde{X}\,^2B_1$)	0.0035	0.0108	0.0000	0.0000	0.0000	0.0000	0.0000
3	$^1A_1$	H$^+$ H$_2$O($\tilde{X}\,^1A_1$)	0.5513	1.5665	1.2960	1.4970	1.3880	1.4080	1.0430
4	$^3A_1$	H(1s) H$_2$O^{+*}($^2A_1$)	2.3717	2.4161	2.4390	2.4500	2.4460	2.4470	2.1300
5	$^1A_1$	H(1s) H$_2$O^{+*}($^2A_1$)	2.5102	3.0279	2.4390	2.4500	2.4460	2.4470	2.1300
6	$^3B_2$	H(1s) H$_2$O^{+*}($^2B_2$)	6.0979	5.9543	6.0190	5.9920	6.0070	6.0040	5.9400
7	$^1B_2$	H(1s) H$_2$O^{+*}($^2B_2$)	6.1011	5.9646	6.0190	5.9920	6.0070	6.0040	5.9400
8	$^3B_1$	H$^+$ H$_2$O*($^3B_1$)	9.2026	9.5559	9.3040	9.2620	9.2950	9.2910	7.0000
9	$^1B_1$	H$^+$ H$_2$O*($^1B_1$)	9.8144	10.170	9.9090	9.8630	9.8980	9.8940	7.4000
10	$^3A_1$	H$^+$ H$_2$O*($^3A_1$)	11.992	12.135	11.847	11.776	11.816	11.809	9.3000
11	$^1A_1$	H$^+$ H$_2$O*($^1A_1$)	13.005	13.248	12.905	12.882	12.882	12.876	9.7000
12	$^3B_2$	H$^+$ H$_2$O*($^3B_2$)	14.192	14.302	14.196	14.154	14.172	14.169	11.040
13	$^1B_2$	H$^+$ H$_2$O*($^1B_2$)	15.191	15.018	14.950	14.886	14.909	14.902	11.050
14	$^3B_2$	H$^+$ H$_2$O*($^3B_2$)	15.017	15.341	14.982	14.960	14.973	14.971	11.410
15	$^1B_2$	H$^+$ H$_2$O*($^1B_2$)	15.683	16.380	15.882	15.879	15.891	15.890	11.500
16	$^3B_1$	H(1s) H$_2$O^{+*}($^4B_1$)	15.770	15.505	15.982	16.023	16.003	16.007	14.778
17	$^3A_1$	H$^+$ H$_2$O*($^3A_1$)	16.526	17.011	16.642	16.682	16.659	16.663	11.100
18	$^1A_1$	H$^+$ H$_2$O*($^1A_1$)	16.490	16.127	16.642	16.682	16.659	16.663	11.130
19	$^3B_1$	H$^+$ H$_2$O*($^3B_1$)	16.967	17.227	17.198	17.243	17.220	17.225	9.9800
20	$^1B_1$	H$^+$ H$_2$O*($^1B_1$)	17.015	17.440	17.198	17.243	17.220	17.225	10.010

resonance-free energy regions. As we shall see, our results support this assumption.

Subtracting it from the calculated (total) ICEC cross section, σ^{ICEC}, we obtain a cross section due to virtual photon exchange only, $\sigma^{\text{v.ph.}}$. This subtraction is, of course, only approximate and less accurate for R for which both contributions are of a similar size. A more accurate approach would be to perform subtraction at the level of the scattering matrices; this is, however, beyond the scope of this work.

The asymptotic cross section expression derived from analytical scattering theory[2,3] accounts only for the virtual photon exchange contribution. This asymptotic cross section is given by

$$\sigma(E) = \frac{3\hbar^4 c^2}{8\pi m_e} \frac{g_A}{g_{A^+}} \frac{\sigma_{PI}^{(A)}(E)\sigma_{PI}^{(N)}(E')}{ER^6 E_{vph}^2}. \tag{2}$$

Here, E and E' are the kinetic energies of the incoming and outgoing electrons, respectively; E_{vph} is the energy of the virtual photon; R is the acceptor–neighbor distance; σ_{PI} are photoionization cross sections for the acceptor, A, and neighbor, N; and g are statistical weights. This cross section can be easily calculated using the available data for the photoionization cross sections. Here, we have used both total photoionization cross sections[27,28] and state-specific data for water.[29]

III. RESULTS AND DISCUSSION

Below, we present and analyze the cross sections for ICEC-P and ICEC-W, for both geometries studied and for several values of R defined as the distance between H/H$^+$ and the oxygen in H_2O^+/H_2O. We also investigate the role of the projectile by comparing electron- and positron-induced electron transfer.

A. Virtual photon vs electron transfer mechanisms

In ICEC-P, the system is initially in the H$^+$ + H_2O ($\tilde{X}$ $^1A_1$) state. Asymptotically, this state is ~1 eV above the lowest energy state of the system: H(1s) + H_2O^+ ($\tilde{X}$ $^2B_1$). As a result, the transfer of an electron from the water to the proton is energetically allowed even for zero kinetic energy. As the thresholds in Table I indicate, additional ICEC channels open as the energy increases. This is visible in the ICEC cross section in Fig. 3, where a step-like behavior is observed for R = 3 Å in σ^{ICEC} and $\sigma^{\text{e transfer}}$ at around 1.4 and 2.0 eV, where the $^1A_1$ state H(1s)+ $H_2O^{+*}(3a_1^{-1})$ becomes energetically accessible; there is no obvious step in $\sigma^{\text{v.ph.}}$. In the case of R = 8 Å, Fig. 4, there is no step in either σ^{ICEC} or $\sigma^{\text{v.ph.}}$. The $\sigma^{\text{e transfer}}$ have a (smaller) step, but since they are very small (see below), this does not affect the ICEC cross section.

Electron transfer cannot lead to a change in the spin of the target. This is confirmed when analyzing the contribution of the different channels. Since the initial state of the system is singlet, the contribution to $\sigma^{\text{e transfer}}$ due to final triplet states is negligible. In the case of $\sigma^{\text{v.ph.}}$, singlet and triplet contributions are of the same order of magnitude.

The *ab initio* cross sections in Figs. 3–7 exhibit significant structure, comprising a large number of very fine peaks. These peaks are associated with resonances (some are actually too narrow to be visible in the curves given the energy grid used). In most cases, these resonances correspond to H_2O Rydberg states, and one
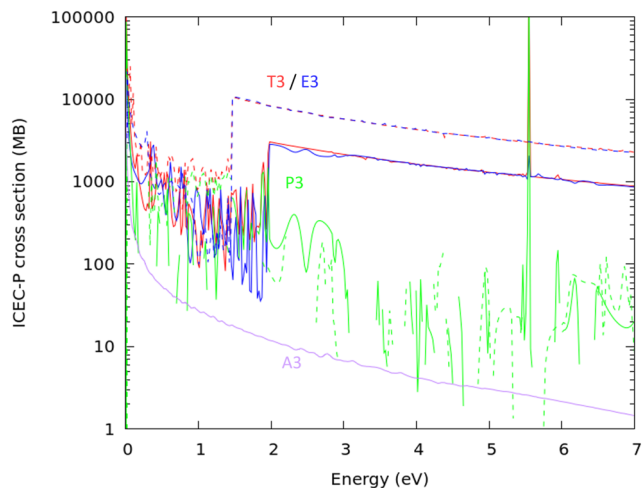

FIG. 3. ICEC-P: cross sections for H_2O–H (solid lines) and H–H_2O (dashed lines) and R = 3 Å. Shown are the total cross section, σ^{ICEC} (T, red line), the electron transfer cross section, $\sigma^{\text{e transfer}}$ (E, blue line), and the virtual photon cross section, $\sigma^{\text{v.ph.}}$ (P, green line). The ICEC cross section obtained with the asymptotic formula is labeled A3, lilac line. Note that in this figure, we have shifted the data so that for each R and geometry, the 0 eV of scattering energy corresponds to the energy of the appropriate initial state.

can see the Rydberg series converging to the thresholds for the H + H_2O^+ states. A few of the resonances, however, correspond to ion pair states.[15] Some of the structures in $\sigma^{\text{v.ph.}}$ are clearly nonphysical. The resonances can appear slightly shifted in σ^{ICEC} and $\sigma^{\text{e transfer}}$. As a result, when subtracting the two to obtain $\sigma^{\text{v.ph.}}$, additional structures appear in the cross sections.
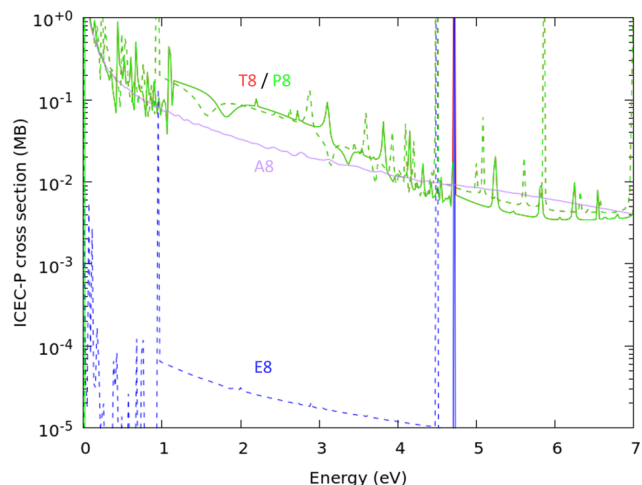

FIG. 4. ICEC-P: cross sections for H_2O–H (solid lines) and H–H_2O (dashed lines) and R = 8 Å. All colors and labels as in Fig. 3. Note that in this figure, we have again shifted the data so that for each R and geometry, the 0 eV of scattering energy corresponds to the energy of the appropriate initial state. Note also that the full and dashed red lines are not visible under the full and dashed green lines respectively.
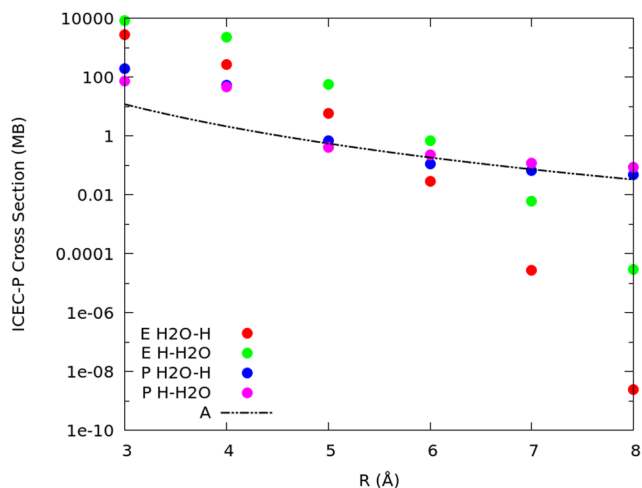
FIG. 5. ICEC-P: $\sigma^{\text{e transfer}}$ (red and green dots) and $\sigma^{\text{v.ph.}}$ (blue and pink dots) as a function of R for E = 2.0 eV and for H_2O–H and H–H_2O. The asymptotic cross section is also included (black line).

FIG. 6. ICEC-W: Cross sections for R = 3 Å for H_2O–H (solid lines) and H–H_2O (dashed lines). All colors and labels as in Fig. 3.

We see in Fig. 4 that for R = 8 Å, $\sigma^{\text{v.ph.}} \simeq \sigma^{\text{ICEC}}$. Electron transfer (blue curves) is significantly smaller (<10^{-3} Mb). Meanwhile, when the distance is reduced to R = 3 Å, $\sigma^{\text{e transfer}} \simeq \sigma^{\text{ICEC}}$, and it is the virtual photon exchange cross section that is smaller, as can be seen in Fig. 3. This is expected, as $\sigma^{\text{v.ph.}}$ is proportional[2,3] to ~R^{-6}, whereas $\sigma^{\text{e transfer}}$ requires orbital overlap and, therefore, depends exponentially on R. This dependence is illustrated in Fig. 5, where we have plotted both cross sections as a function of R for ICEC-P (the results for ICEC-W are similar) and a kinetic energy of 2 eV. The much faster decrease of $\sigma^{\text{e transfer}}$ as R increases is clearly visible, as is the effect of the orientation on this cross section. As expected, the agreement of $\sigma^{\text{v.ph.}}$ with the asymptotic cross section is better at bigger R.

As expected, $\sigma^{\text{v.ph.}}$ agrees better with the cross section given by the asymptotic formula for larger R, although the resonances make it hard to see this in detail, and fairly independent of geometry (i.e., where H/H^+ is located with respect to H_2O/H_2O^+). The asymptotic formula corresponds to averaging over the orientations of the molecule. Meanwhile, $\sigma^{\text{e transfer}}$ is quite sensitive to the geometry, and this sensitivity increases as R increases: whereas the difference between geometries for R = 3 Å is less than an order of magnitude, in the case of R = 8 Å, the difference is around five orders of magnitude. We interpret this to be due to the sensitivity of the electron transfer to the overlap between acceptor and neighbor wavefunctions: at larger distances where this overlap is very small, the orientation of the molecule with respect to H/H^+ has a stronger effect on the electron transfer. Despite this dependence, geometry has hardly any effect on σ^{ICEC} at R = 8 Å, where the main contribution to ICEC is due to virtual photon exchange, but makes a difference for R = 3 Å, where the main contribution is due to electron transfer. $\sigma^{\text{e transfer}}$ is bigger for H–H_2O, indicating that a transfer of the electron is more likely when H^+ is on the side of the H of water rather than that of O.

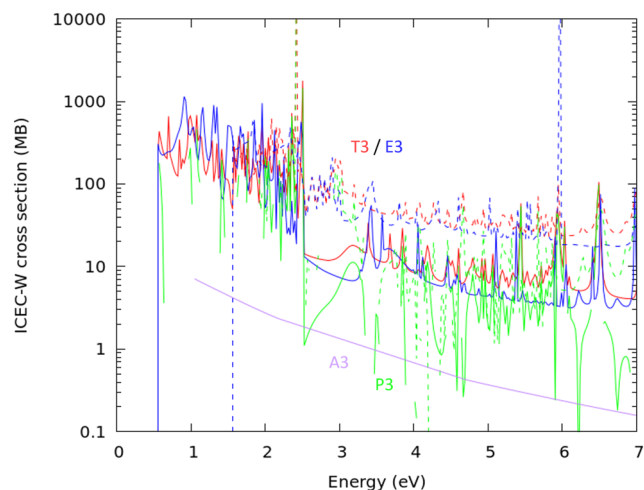We now discuss the ICEC-W cross sections, plotted in Figs. 6 and 7: in this case, the degenerate initial state H(1s)+ $H_2O^+(1b_1^{-1})$ is the lowest state of the system. Therefore, there is a threshold for ICEC. However, since there is only one possible final state of the ICEC process in the energy range of interest, there are no step-like features in the cross sections.

We see in Fig. 7 that for R = 8 Å, again $\sigma^{\text{v.ph.}} \simeq \sigma^{\text{ICEC}}$ and $\sigma^{\text{e transfer}} < 10^{-7}$ Mb. However, although for R = 3 Å, we again find that $\sigma^{\text{e transfer}} \simeq \sigma^{\text{ICEC}}$ (see Fig. 6), $\sigma^{\text{v.ph.}}$ contributes a larger proportion than for ICEC-P despite being smaller in absolute value. This is not surprising: the transfer of an electron is not energetically favorable in this case, so one would expect $\sigma^{\text{e transfer}}$ to be smaller than for ICEC-P. The process, therefore, contributes proportionally less
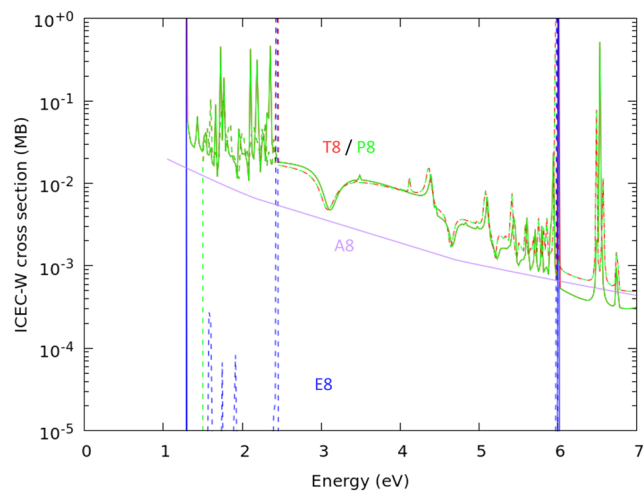

FIG. 7. ICEC-W: Cross sections for R = 8 Å for H_2O–H (solid lines) and H–H_2O (dashed lines). All colors and labels as in Fig. 3.
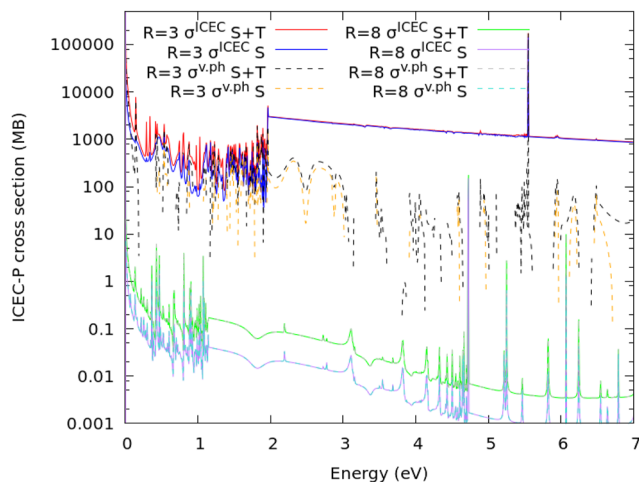
FIG. 8. ICEC-P: $\sigma^{\text{v.ph.}}$ and σ^{ICEC} for R = 3 and 8 Å calculated including (curves labeled S + T) and excluding (curves labeled S) the contribution of triplet final states. For 8 Å, $\sigma^{\text{v.ph.}}$ are not visible as they sit under σ^{ICEC}.

to the total cross section. This also explains why the ICEC-W cross section is smaller than the ICEC-P one, particularly for small R where the electron transfer is very effective for ICEC-P: although $\sigma^{\text{v.ph.}}$ is also smaller for ICEC-W, the difference in magnitude is larger for $\sigma^{\text{e transfer}}$. The effect of geometry is similar to that for ICEC-P, with the largest difference between geometries occurring for $\sigma^{\text{e transfer}}$ for R = 8 Å.

Since electron transfer only produces singlet final states, we would expect that for R = 3 Å, where $\sigma^{\text{e transfer}} \simeq \sigma^{\text{ICEC}}$, singlet states are almost exclusively produced. This is not the case for R = 8 Å. In other words, the proportion of singlet and triplet states produced as

a result of ICEC is R dependent. This is illustrated in Fig. 8, where we have plotted, for ICEC-P, σ^{ICEC} and $\sigma^{\text{v.ph.}}$ calculated including and excluding the contribution of triplet final states for R = 3 and 8 Å. For R = 3 Å, σ^{ICEC} barely changes if the triplets are excluded because its largest contribution is due to electron transfer. The differences visible in $\sigma^{\text{v.ph.}}$ have little effect on it. This confirms that it is almost exclusively singlet states that would be produced. In the case of R = 8 Å, the differences in σ^{ICEC} when the triplets are excluded are close to an order of magnitude, confirming that both singlet and triplet final states would be produced in significant numbers. For this R, the contribution of electron transfer is negligible: the $\sigma^{\text{v.ph.}}$ are not visible in the figure because they sit exactly under σ^{ICEC}. This differential production of singlets and triplets is particularly interesting in the case of ICEC-W where singlet and triplet final states correspond to the singlet and triplet states of H_2O.

Again, we see in Fig. 7 that the cross section determined with the asymptotic formula agrees well with $\sigma^{\text{v.ph.}}$. In ICEC-W, we only consider ICEC for H_2O^+ in its initial ground state, $^2B_1$. Therefore, the consistent asymptotic cross section includes the photoionization cross section for the final state H_2O^+ ($\tilde{X}\,^2B_1$) only. The theoretical photoionization cross sections used underestimate the experiment, which could partially explain why the analytical cross section is smaller than $\sigma^{\text{v.ph.}}$.

As seen in the figures, the asymptotic formula gives cross sections smaller than our $\sigma^{\text{v.ph.}}$ for the whole scattering energy range for R = 3 Å. For R = 8 Å, the asymptotic formula gives cross sections that are closer to the calculated $\sigma^{\text{v.ph.}}$, as expected, although higher for energies above ~4.5 eV for ICEC-P and ~6 eV for ICEC-W.

Figure 9 shows the ratio $\sigma^{\text{v.ph.}}/\sigma^{\text{e transfer}}$ for ICEC-P for the range of R investigated. The ratio is larger for bigger R; as R decreases, the likelihood of electron transfer increases faster than that of virtual photon exchange: R = 6 Å seems to be the "transition" distance for which the contribution of electron transfer becomes bigger than that of the photon exchange. In fact, at R = 6 Å, the H_2O–H ratio is

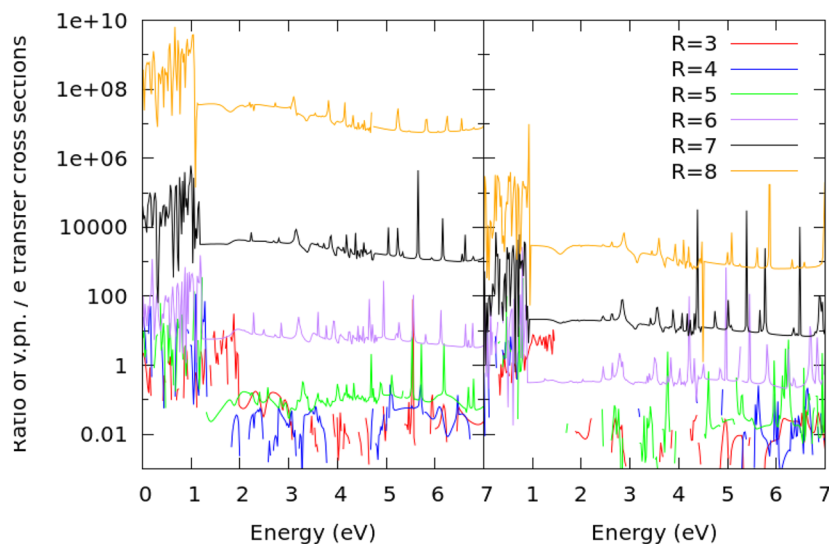**FIG. 9.** ICEC-P: Ratio $\sigma^{\text{v.ph.}}/\sigma^{\text{e transfer}}$ for R = 3–8 Å. Left panel: H_2O–H; right panel: H–H_2O. The data are shifted as in Figs. 3 and 4.
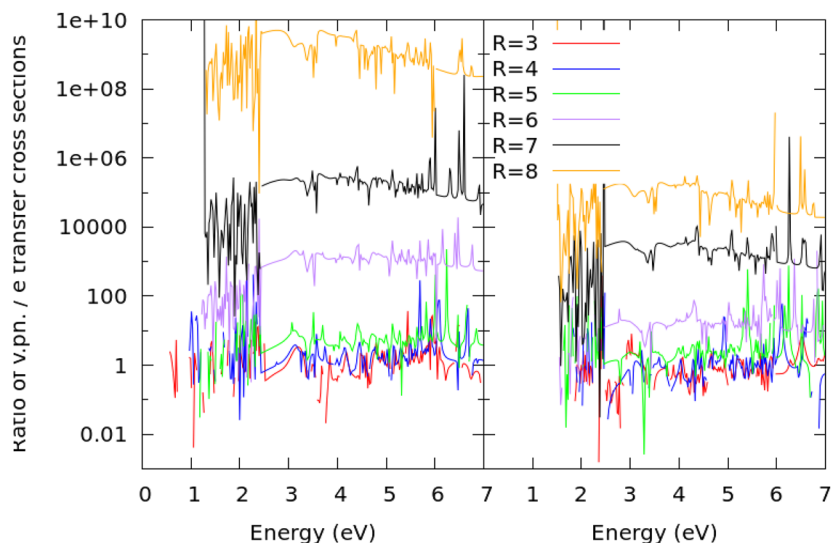
31 May 2024 11:15:29

FIG. 10. ICEC-W: Ratio $\sigma^{v.ph.}/\sigma^{e\ transfer}$ for R = 3–8 Å. Left panel: H_2O–H; right panel: H–H_2O.

greater than 1, but the H–H_2O one is smaller than 1, confirming that (at R ≤ 6 Å at least) it is easier for an electron to be transferred from H_2O to H^+ if H^+ is situated on the H end of water. For both geometries, $\sigma^{v.ph.}$ is of similar size and very similar to the asymptotic cross section, whereas $\sigma^{e\ transfer}$ differs by around two orders of magnitude.

We clearly see that the geometry effect on the ratio is more significant for large R. This is due to the strong geometry effect on $\sigma^{e\ transfer}$ when R increases, in contrast to the negligible effect on $\sigma^{v.\ ph.}$ for all R. We note that this geometry dependence at large R is likely to be quite sensitive to the description of the orbitals of H and H_2O: changes to the choice of basis set and orbital may affect the comparison.

The same ratios are presented for ICEC-W in Fig. 10. Here, no superelastic scattering is possible (i.e., the electron transfer is not energetically allowed at 0 eV of kinetic energy), so, instead, the cross sections converge to ~1 as R decreases. This indicates that in ICEC-W, as R decreases, electron transfer becomes more likely, but not more likely than virtual photon exchange.

B. Role of the projectile in electron transfer

It is interesting to attempt to ascertain the role the projectile plays in the electron transfer process. In ICEC-P, there is no need for the projectile to "contribute" any kinetic energy in order for the electron transfer to be energetically allowed (in this fixed-nuclei picture, the process is superelastic and the scattering electron leaves with more energy). In ICEC-W, around 1 eV needs to be deposited: there is no electron transfer (in fact, no ICEC) below this scattering energy. The rate at which $\sigma^{e\ transfer}$ decreases as the scattering energy increases is similar for both systems, perhaps slightly faster for ICEC-W. This indicates that the projectile is not completely passive as its kinetic energy affects the electron transfer, but this effect seems not to be very dependent on the specific process.

To gain more insights into the role of the projectile, we have run the same calculations (i.e., using the same target and scattering models) for positron scattering, that is, changing the charge of the projectile. In this case, our calculations only model the electron transfer process. Neither positronium formation nor a potential positron capture (positron binding) that would lead to ionization of the environment can be modeled with the UKRmol+ suite.

Figure 11 shows the ratio of the electron- and positron-induced electron transfer cross section for two R and both ICEC-W and ICEC-P. The ratio is bigger for smaller R, particularly at low energies, but we do not see a strong geometry dependence. The
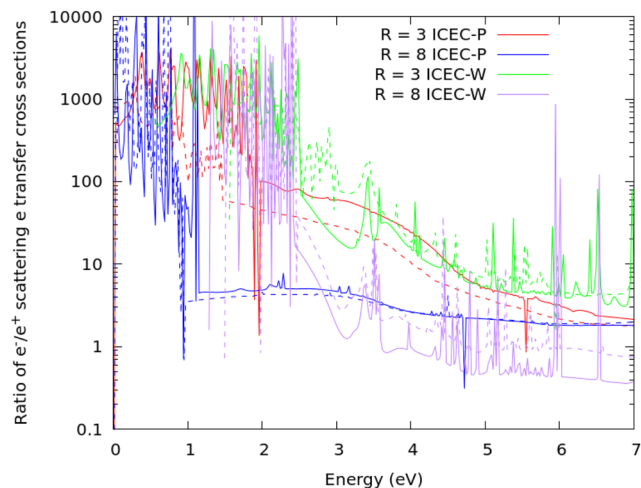

FIG. 11. Ratio of electron- and positron-induced electron transfer cross sections for R = 3 and 8 Å for ICEC-P and ICEC-W for H_2O–H (solid lines) and H–H_2O (dashed lines).

dependence on the scattering energy is stronger for small R. Finally, ICEC-P leads, on the whole, to a larger ratio above ~2.5 eV, in particular for the larger R. These dependencies point at the projectile not having a passive role: its interaction with the whole system seems to affect the electron transfer process.

For R = 8 Å, the ratio is above 2 for the whole energy range for ICEC-P, whereas for ICEC-W, it is close or below 1 above ~3 eV. (The overall behavior of the ratio below ~2.4 eV is hard to ascertain due to the resonances present.) For R = 3 Å, conversely, the ratio is 100 and bigger below ≃2.5 eV, decreasing perhaps toward 2 as the energy increases for both ICEC-P and ICEC-W. It should be noted that the accuracy of the ratios is dependent on modeling positron than electron scattering similarly well. However, R-matrix calculations are poorer at modeling positron than electron scattering. Using the same model for both projectiles, as we have done here, can lead to results of poorer quality in the case of positrons and underestimated elastic cross sections at low energies.[30] The apparent convergence of the ratios to 2 for three out of the four cases plotted could, therefore, point at our calculations underestimating the positron-induced electron transfer rather than at a physical effect. What is clear is that as the energy increases the ratio becomes less energy dependent and that the charge of the projectile has a more significant effect for small R. It is not obvious why the effect of the charge of the projectile is dependent on the geometry of the target.

IV. CONCLUSION

Using the R-matrix approach, we have calculated ICEC cross sections for $H^+ + H_2O$ and $H + H_2O^+$ and disentangled the contributions of electron transfer and virtual photon exchange as a function of the distance between acceptor and neighbor and their relative orientation. We have shown that, as expected, electron transfer makes the largest contribution to the ICEC cross section at smaller R. We have also shown that, for the cases studied, the difference between the cross section obtained by the asymptotic formula and the *ab initio* ICEC cross section is due, in most cases, almost completely to the electron transfer process. The electron transfer mechanism, which can be seen as an electron capture by the acceptor from its neighbor rather than the continuum, is significant for a range of acceptor–neighbor distances. One should ensure that studies of ICEC process make it clear whether one or both mechanisms are being investigated or modeled.

We have shown that, for the systems studied, the magnitude of the electron transfer cross section depends strongly on the relative position of acceptor and neighbor, whereas the photon transfer process depends on the distance between acceptor and donor but is fairly insensitive to their relative orientation. Although the orientation dependence of $\sigma^{e\ transfer}$ is stronger for larger R, its smaller contribution to σ^{ICEC} means that the latter cross section is more orientation dependent for small R. In addition, $\sigma^{e\ transfer}$ is responsible in ICEC-P for the step-like behavior of σ^{ICEC}, which is due to final channels becoming energetically accessible; $\sigma^{v.ph.}$ has a smooth dependence with energy.

The electron transfer mechanism cannot lead to changes to the spin of the target, whereas the virtual photon exchange does. This differential production of triplet and singlet state points at a potential way of establishing, for some systems, whether virtual photon exchange takes place. For example, in the case of ICEC-W, electron transfer cannot lead to the production of H_2O in a triplet state. The channels associated with the first singlet and triplet excited states of water become energetically available above 9.3–9.9 eV (see Table I). If one could experimentally determine the state of the neutral water produced in the process for electron energies above ~10 eV, the presence of triplet states would confirm that virtual photon exchange is taking place. In addition, due to the dependence of the cross sections with R, a higher proportion of triplet states are produced when the electron transfer contributes relatively less to the process, in other words, when the distance between acceptor and neighbor is large.

A comparison of the two systems investigated, $H^+ + H_2O$ and $H + H_2O^+$, shows that both $\sigma^{e\ transfer}$ and $\sigma^{v.ph.}$ are sensitive to the energetics of the system. For small R, the total cross section for ICEC-W is smaller because the dominant electron transfer is smaller as there are fewer open channels than in ICEC-P. For large R, the virtual photon cross section dominates, and this is also smaller for ICEC-W. We can understand this for the cross section given by the asymptotic formula in terms of the size of photorecombination and photoionization cross section included. The photoionization cross section for H_2O required in ICEC-P, which includes contributions of several final cationic channels, is much larger than the photorecombination one needed for ICEC-W for most of the energy range.

We have looked at the effect of the charge of the projectile on the electron transfer process by comparing electron and positron scattering. We have shown that this effect is significant for low scattering energy but gets smaller as this energy increases. The dependence of the ratio on the distance between acceptor and neighbor at low energies could be related to how the positive/negative charge of the projectile affects the charge distribution in the target systems.

Our results point at the importance of *ab initio* calculations in the study of ICEC and for comparison with experiment, especially if the electron transfer and virtual photon exchange contributions cannot be separated. Neither orientation effects nor those due to channel opening are accounted for by the asymptotic formula. Although the effect of the geometry of water is still to be studied, the present results show a strong dependence of the cross section on geometry. This has implications for ICEC in environments of applied relevance, where there are usually many environment particles. Earlier work on ICEC for $Ne^+–He$ and $Ne^+–He_2$ showed approximate additivity of the cross section;[13] even if this applied for the systems studied here, consideration of the relative orientation of the neighbors with respect to the acceptor would require the determination of single neighbor cross sections for a range of orientations. The dependence of the cross sections on geometry also points at the importance, already observed for ICD, of going beyond a fixed-nuclei picture and considering nuclear dynamics in ICEC.

31 May 2024 11:15:29

AUTHOR DECLARATIONS

Conflict of Interest

The authors have no conflicts to disclose.

Author Contributions

Vincent Graves: Formal analysis (equal); Investigation (lead); Software (lead); Writing – original draft (equal); Writing – review & editing (supporting). **Jan Šenk**: Formal analysis (supporting); Writing – original draft (supporting); Writing – review & editing (supporting). **Přemysl Kolorenč**: Formal analysis (supporting); Writing – original draft (supporting); Writing – review & editing (supporting). **Nicolas Sisourat**: Conceptualization (equal); Formal analysis (equal); Writing – original draft (supporting); Writing – review & editing (supporting). **Jimena D. Gorfinkiel**: Conceptualization (equal); Formal analysis (equal); Funding acquisition (lead); Methodology (equal); Resources (lead); Writing – original draft (equal); Writing – review & editing (lead).

DATA AVAILABILITY

The data that support the findings of this study are openly available in the Open University's research data repository at https://doi.org/10.21954/ou.rd.25569066.v2.

REFERENCES

[1] A. Bande, E. Fasshauer, A. Molle, D. Peláez, F. M. Pont, and N. Sisourat, "Interatomic coulombic electron capture: The story so far," J. Phys. B: At., Mol. Opt. Phys. **56**, 232001 (2023).

[2] K. Gokhberg and L. S. Cederbaum, "Environment assisted electron capture," J. Phys. B: At., Mol. Opt. Phys. **42**, 231001 (2009) theory.

[3] K. Gokhberg and L. S. Cederbaum, "Interatomic Coulombic electron capture," Phys. Rev. A **82**, 052707 (2010) theory.

[4] J. D. Gorfinkiel and S. Ptasińska, "Electron scattering from molecules and molecular aggregates of biological relevance," J. Phys. B: At., Mol. Opt. Phys. **50**, 182001 (2017).

[5] T. Jahnke, U. Hergenhahn, B. Winter, R. Dörner, U. Frühling, P. V. Demekhin, K. Gokhberg, L. S. Cederbaum, A. Ehresmann, A. Knie, and A. Dreuw, "Interatomic and intermolecular Coulombic decay," Chem. Rev. **120**, 11295–11369 (2020).

[6] V. Averbukh, I. B. Müller, and L. S. Cederbaum, "Mechanism of interatomic Coulombic decay in clusters," Phys. Rev. Lett. **93**, 263002 (2004) theory.

[7] T. Jahnke, A. Czasch, M. Schöffler, S. Schössler, M. Käsz, J. Titze, K. Kreidi, R. E. Grisenti, A. Staudte, O. Jagutzki, L. Schmidt, T. Weber, H. Schmidt-Böcking, K. Ueda, and R. Dörner, "Experimental separation of virtual photon exchange and electron transfer in interatomic Coulombic decay of neon dimers," Phys. Rev. Lett. **99**, 153401 (2007).

[8] J. Rist, T. Miteva, B. Gaire, H. Sann, F. Trinter, M. Keiling, N. Gehrken, A. Moradmand, B. Berry, M. Zohrabi, M. Kunitski, I. Ben-Itzhak, A. Belkacem, T. Weber, A. L. Landers, M. Schöffler, J. B. Williams, P. Kolorenč, K. Gokhberg, T. Jahnke, and R. Dörner, "A comprehensive study of Interatomic Coulombic Decay in argon dimers: Extracting R-dependent absolute decay rates from the experiment," Chem. Phys. **482**, 185 (2017).

[9] L. Ben Ltaief, M. Shcherbinin, S. Mandal, S. R. Krishnan, A. C. LaForge, R. Richter, S. Turchini, N. Zema, T. Pfeifer, E. Fasshauer, N. Sisourat, and M. Mudrich, "Charge exchange dominates long-range interatomic Coulombic decay of excited metal-doped helium nanodroplets," J. Phys. Chem. Lett. **10**, 6904 (2019).

[10] P. G. Burke, *R-Matrix Theory of Atomic Collisions: Application to Atomic, Molecular and Optical Processes* (Springer, 2011).

[11] J. Tennyson, "Electron–molecule collision calculations using the R-matrix method," Phys. Rep. **491**, 29–76 (2010).

[12] Z. Mašín, J. Benda, J. D. Gorfinkiel, A. G. Harvey, and J. Tennyson, "UKRmol+: A suite for modelling electronic processes in molecules interacting with electrons, positrons and photons using the R-matrix method," Comput. Phys. Commun. **249**, 107092 (2020).

[13] N. Sisourat, T. Miteva, J. D. Gorfinkiel, K. Gokhberg, and L. S. Cederbaum, Phys. Rev. A **98**, 020701 (2018).

[14] A. Molle, A. Dubois, J. D. Gorfinkiel, L. S. Cederbaum, and N. Sisourat, "Electron attachment to a proton in water by interatomic coulombic electron capture: An R-matrix study," Phys. Rev. A **104**, 022818 (2021).

[15] A. Molle, A. Dubois, J. D. Gorfinkiel, L. S. Cederbaum, and N. Sisourat, "Fano interferences in environment-enabled electron capture," Phys. Rev. A **103**, 012808 (2021).

[16] K. L. Baluja, R. Zhang, J. Franz, and J. Tennyson, "Low-energy positron collisions with water: Elastic and rotationally inelastic scattering," J. Phys. B: At., Mol. Opt. Phys. **40**, 3515–3524 (2007).

[17] D. Edwards, D. Stevens, Z. Cheong, V. Graves, J. D. Gorfinkiel, F. Blanco, G. Garcia, M. J. Brunger, R. D. White, and J. P. Sullivan, "Positron scattering from pyrazine," Phys. Rev. A **104**, 042807 (2021).

[18] H.-J. Werner, P. J. Knowles, P. Celani, W. Györffy, A. Hesselmann, D. Kats, G. Knizia, A. Köhn, T. Korona, D. Kreplin, R. Lindh, Q. Ma, F. R. Manby, A. Mitrushenkov, G. Rauhut, M. Schütz, K. R. Shamasundar, T. B. Adler, R. D. Amos, S. J. Bennie, A. Bernhardsson, A. Berning, J. A. Black, P. J. Bygrave, R. Cimiraglia, D. L. Cooper, D. Coughtrie, M. J. O. Deegan, A. J. Dobbyn, K. Doll, M. Dornbach, F. Eckert, S. Erfort, E. Goll, C. Hampel, G. Hetzer, J. G. Hill, M. Hodges, T. Hrenar, G. Jansen, C. Köppl, C. Kollmar, S. J. R. Lee, Y. Liu, A. W. Lloyd, R. A. Mata, A. J. May, B. Mussard, S. J. McNicholas, W. Meyer, T. F. Miller III, M. E. Mura, A. Nicklass, D. P. O'Neill, P. Palmieri, D. Peng, K. A. Peterson, K. Pflüger, R. Pitzer, I. Polyak, M. Reiher, J. O. Richardson, J. B. Robinson, B. Schröder, M. Schwilk, T. Shiozaki, M. Sibaev, H. Stoll, A. J. Stone, T. Tarroni, T. Thorsteinsson, J. Toulouse, M. Wang, M. Welborn, and B. Ziegler, MOLPRO, *version, a package of ab initio programs*, https://www.molpro.net.

[19] O. Dutuit, A. Tabche-Fouhaile, I. Nenner, H. Frohlich, and P. M. Guyon, "Photodissociation processes of water vapor below and above the ionization potential," J. Chem. Phys. **83**, 584–596 (1985).

[20] Z.-L. Cai, D. J. Tozer, and J. R. Reimers, "Time-dependent density-functional determination of arbitrary singlet and triplet excited-state potential energy surfaces: Application to the water molecule," J. Chem. Phys. **113**, 7084–7096 (2000).

[21] D. H. Katayama, R. E. Huffman, and C. L. O'Bryan, "Absorption and photoionization cross sections for H_2O and D_2O in the vacuum ultraviolet," J. Chem. Phys. **59**, 4309–4319 (1973).

[22] A. Chutjian, R. I. Hall, and S. Trajmar, "Electron-impact excitation of H_2O and D_2O at various scattering angles and impact energies in the energy-loss range 4.2–12 eV," J. Chem. Phys. **63**, 892–898 (1975).

[23] M. Rubio, L. Serrano-Andrés, and M. Merchán, "Excited states of the water molecule: Analysis of the valence and Rydberg character," J. Chem. Phys. **128**, 104305 (2008).

[24] P. Modak and B. Antony, "Probing photon interaction with H_2O and D_2O," J. Phys. B: At., Mol. Opt. Phys. **53**, 045202 (2020).

[25] H. Bachau, E. Cormier, P. Decleva, J. E. Hansen, and F. Martin, Rep. Prog. Phys. **64**, 1815–1943 (2001).

[26] J. M. Carr, P. G. Galiatsatos, J. D. Gorfinkiel, A. G. Harvey, M. A. Lysaght, D. Madden, Z. Mašín, M. Plummer, J. Tennyson, and H. N. Varambhia, "UKRmol: A low-energy electron- and positron-molecule scattering suite," Eur. Phys. J. D **66**, 58 (2012).

[27] A. N. Heays, A. D. Bosman, and E. F. van Dishoeck, "Photodissociation and photoionisation of atoms and molecules of astrophysical interest," Astron. Astrophys. **602**, A105 (2017).

[28]"Leiden database for photodissociation and photoionization of astrophysically relevant molecules," https://home.strw.leidenuniv.nl/~ewine/photo/cross_sections.html.

[29]J. Benda, J. D. Gorfinkiel, Z. Mašín, G. S. J. Armstrong, A. C. Brown, D. D. A. Clarke, H. W. van der Hart, and J. Wragg, "Perturbative and nonperturbative photoionization of H_2 and H_2O using the molecular R-matrix-with-time method," Phys. Rev. A **102**, 052826 (2020).

[30]V. Graves and J. D. Gorfinkiel, "R-matrix calculations for elastic electron and positron scattering from pyrazine: Effect of the polarization description," Eur. Phys. J. D **76**, 43 (2022).

31 May 2024 11:15:29